





RESEARCH ARTICLE

Neuronal density and expression of calcium-binding proteins across the layers of the superior colliculus in the common marmoset (*Callithrix jacchus*)

Melissa H. Y. Chong  | Katrina H. Worthy  | Marcello G. P. Rosa  |
Nafiseh Atapour 

Department of Physiology and Neuroscience
Program, Biomedicine Discovery Institute,
Monash University, Melbourne, Australia

Correspondence

Nafiseh Atapour, Department of Physiology
and Neuroscience Program, Biomedicine
Discovery Institute, Monash University,
Melbourne, VIC 3800, Australia.
Email: nafiseh.atapour@monash.edu

Funding information

National Health and Medical Research Council
(APP1194206) to Marcello G. P. Rosa.

Abstract

The superior colliculus (SC) is a layered midbrain structure with functions that include polysensory and sensorimotor integration. Here, we describe the distribution of different immunohistochemically identified classes of neurons in the SC of adult marmoset monkeys (*Callithrix jacchus*). Neuronal nuclei (NeuN) staining was used to determine the overall neuronal density in the different SC layers. In addition, we studied the distribution of neurons expressing different calcium-binding proteins (calbindin [CB], parvalbumin [PV] and calretinin [CR]). Our results indicate that neuronal density in the SC decreases from superficial to deep layers. Although the neuronal density within the same layer varies little across the mediolateral axis, it tends to be lower at rostral levels, compared to caudal levels. Cells expressing different calcium-binding proteins display differential gradients of density according to depth. Both CB- and CR-expressing neurons show markedly higher densities in the stratum griseum superficiale (SGS), compared to the stratum opticum and intermediate and deep layers. However, CR-expressing neurons are twice as common as CB-expressing neurons outside the SGS. The distribution of PV-expressing cells follows a shallow density gradient from superficial to deep layers. When normalized relative to total neuronal density, the proportion of CR-expressing neurons increases between the superficial and intermediate layers, whereas that of CB-expressing neurons declines toward the deep layers. The proportion of PV-expressing neurons remains constant across layers. Our data provide layer-specific and accurate estimates of neuronal density, which may be important for the generation of biophysical models of how the primate SC transforms sensory inputs into motor signals.

KEYWORDS

calcium-binding proteins, immunostaining, neuronal density, primate, superior colliculus

This is an open access article under the terms of the [Creative Commons Attribution-NonCommercial-NoDerivs](https://creativecommons.org/licenses/by-nc-nd/4.0/) License, which permits use and distribution in any medium, provided the original work is properly cited, the use is non-commercial and no modifications or adaptations are made.

© 2022 The Authors. *The Journal of Comparative Neurology* published by Wiley Periodicals LLC.

1 | INTRODUCTION

The superior colliculus (SC) is a midbrain structure with roles that include the coordination of eye, neck, and shoulder movement to dynamically respond to novel stimuli (Allen et al., 2021; White & Munoz, 2012). The SC is a key locus for integrating and converting many types of sensory information (e.g., visual, auditory, somatosensory) into movement signals (Allen et al., 2021; Chen et al., 2019; Corneil & Munoz, 2014; Isa et al., 2021; White & Munoz, 2012). The present study addresses the neuronal composition of the SC in the common marmoset monkey (*Callithrix jacchus*), one of the smallest simian primates.

Histologically, the SC consists of seven distinct cellular layers, which are typically regarded as being organized into three functional regions (Baldwin & Krubitzer, 2018; May, 2006). The three dorsal-most layers (stratum zonale [SZ], stratum griseum superficiale [SGS] and stratum opticum [SO]) form the superficial functional region, which receives and processes visual input (Corneil & Munoz, 2014; Rosa & Schmid, 1994). The intermediate (stratum griseum intermedium [SGI] and stratum album intermedium [SAI]) and deep (stratum griseum profundum [SGP] and stratum album profundum [SAP]) functional regions facilitate higher-level processes such as the integration of convergent sensory, cognitive, and motor-related information (Corneil & Munoz, 2014; White & Munoz, 2012).

The SC comprises a heterogeneous neuronal population composed of inhibitory and excitatory projection neurons intermingled with local interneurons (Bourne & Rosa, 2003; Essig et al., 2021; Hilbig et al., 1999; Laemle, 1981; Ma et al., 1990; Mize, 1992; Sooksawat et al., 2011; White & Munoz, 2012; Whyland et al., 2020). The calcium-binding proteins calbindin (CB), calretinin (CR), and parvalbumin (PV) are among the known markers present in some populations of SC neurons (Baldwin & Krubitzer, 2018; Bishop et al., 2012; Kook et al., 2014; McHaffie et al., 2001; Soares et al., 2001). However, studies in primates so far have been based solely on qualitative assessments. In New World titi monkeys, it has been described that the occurrence of CB- and PV-stained neurons decreases gradually from dorsal to ventral layers of the SC (Baldwin & Krubitzer, 2018), whereas observations in *Cebus* monkeys indicate heavy CR and CB staining in the superficial layers and PV staining throughout the SC (Soares et al., 2001). The latter description agrees with the pattern described for Old World macaque monkeys (McHaffie et al., 2001).

The marmoset monkey is an emerging animal model in neuroscience, with interest growing rapidly due to factors including its small size, lissencephalic brain, short developmental cycle and lower biosafety risk compared to macaque monkeys (Solomon & Rosa, 2014; Mitchell & Leopold, 2015; Okano et al., 2012). In the present study, we aimed to quantify the neuronal distribution in the SC of marmosets using stereological analysis of sections stained for a specific neuronal marker, neuronal nuclei (NeuN; Wolf et al., 1996). We further examined the localization of CB-, CR-, and PV-expressing neurons to provide insights into their likely differential contributions to the SC neuronal network.

2 | METHODS

2.1 | Animals

Materials obtained from six healthy adult marmosets (*C. jacchus*) aged between 26 and 43 months (four females; F1741, F1882 and CJ200, CJ167 and two males; CJ195 and CJ205). The experiments were conducted in accordance with the Australian Code of Practice for the Care and Use of Animals for Scientific Purposes. All procedures were approved by the Monash University Animal Ethics Experimentation Committee, which also monitored the health and well-being of the animals throughout the experiments. The animals had no veterinary record of serious or chronic health conditions.

2.2 | Tissue perfusion, preparation, and cryosectioning

At the conclusion of the anatomical tracing experiment unrelated to the present study (Majka et al., 2016, 2020), the marmosets were overdosed using sodium pentobarbitone (100 mg/kg, i.m.), and transcardial perfusion was performed using heparinized saline, followed by 4% paraformaldehyde in 0.1 M phosphate buffer (Atapour et al., 2017). The collected brains were postfixed in the same medium for 24 h, after which cryoprotection was performed by submerging the brains in buffered paraformaldehyde solution containing increasing concentrations of sucrose (10%, 20%, and 30%). Cryosectioning of the hemisphere contralateral to the tracer injections was performed at 40 μ m on a Leica CM1850 cryostat, yielding five sequential series of coronal sections. Different series were stained for different markers including myelin (Gallyas, 1979, modified by Worthy et al., 2017) and NeuN (Wolf et al., 1996) to help delineate the laminar boundaries. Other series were stained for calcium-binding proteins.

2.3 | Immunostaining

The primary antibodies used in this study were specific for NeuN [1:800, Merck Millipore (USA), MAB377, Clone A60, RRID: AB_2298772], CB [1:8000, Swant (Switzerland), Code No. 300, RRID: AB_10000347], CR [1:8000, Swant (Switzerland), Code 6B3pur, RRID: AB_10000320], and PV [1:8000, Swant (Switzerland), Code 235, RRID: AB_10000343]. The sections were incubated in blocking solution (10% normal horse serum and 0.3% Triton-X100 in 0.1 M PB) for 1 h at room temperature before undergoing primary antibody incubation at 4°C for 42–46 h. A biotinylated horse anti-mouse IgG secondary antibody [1:200, PK-6102, Vectastain elite ABC HRP kit, Vector Laboratories (USA), RRID: AB_2336821] incubation was then conducted for 30 min, followed by treatment with Avidin-Biotin Complex reagent (PK-6102). These applications were timed 30 min and conducted at room temperature. DAB substrate working solution (DAB kit SK-4100, RRID: AB_2336382) was then applied.

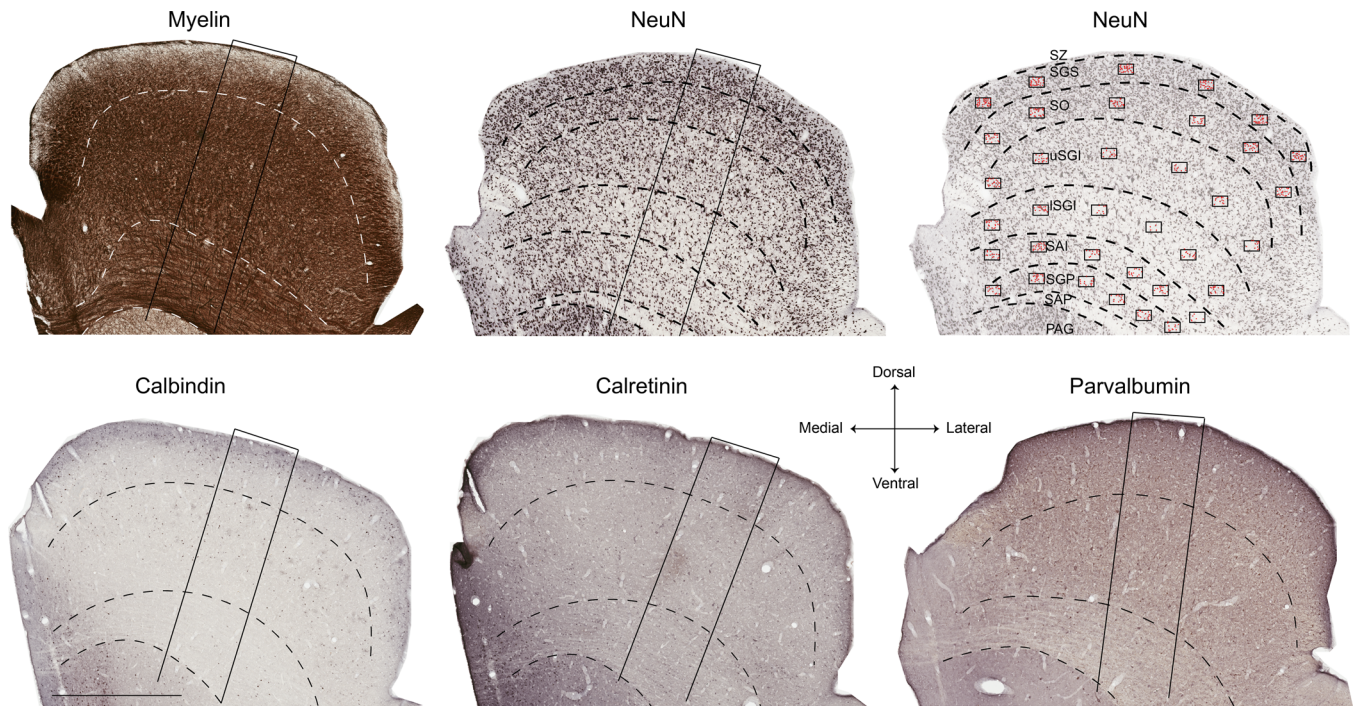


FIGURE 1 Coronal sections of marmoset SC stained for myelin, NeuN (top), and calcium-binding proteins (calbindin, calretinin, and parvalbumin; bottom). Images represent sections from interaural levels near the central part of the SC (Paxinos et al., 2012). Top left: myelin stain; top middle: NeuN stain. Dashed lines indicate the boundaries between the layers of the SC. The oblique rectangles in the myelin and NeuN images indicate the locations of the close-up images shown in Figure 2. Top right: reduced opacity version of the NeuN-stained image, indicating the location of counting frames (black rectangles) and counted neurons (red dots) used in stereological analysis. Bottom: sections stained for different calcium-binding proteins. The oblique rectangles in each image indicate the locations of the close-up images shown in Figure 4. Scale (bottom left): 1 mm. Abbreviations: PAG, periaqueductal gray; SAI, stratum album intermedium; SAP, stratum album profundum; SGP, stratum griseum profundum; SGI, stratum griseum intermedium; SC, superior colliculus; SZ, stratum zonale; SGS, stratum griseum superficiale; SO, stratum opticum

2.4 | Stereological sampling and analysis

An Aperio Scanscope AT Turbo (Leica Biosystems, Germany) was used to scan sections containing the SC ($\times 20$ magnification, resolution: $0.5 \mu\text{m}/\text{pixel}$). Neuronal counts presented in Figures 2 and 4 were obtained from three coronal SC sections $200 \mu\text{m}$ apart, approximately from the central part of the SC (including AP level $+1.0 \text{ mm}$ of Paxinos et al. 2012). As shown in Figure 1, stereological sampling included six counting rectangles (each $150 \times 100 \mu\text{m}^2$) placed equidistant from the lateral to the medial limits of each SC layer, excluding the SZ and SAP, which are primarily composed of myelinated fibers. Our sampling method was similar to that of Williams and Rakic (1988), also used by Finlay et al., 2014 and ourselves (Atapour et al., 2017) in the lateral geniculate nucleus in which radial probes are placed to evenly divide the outer- and innermost perimeters to designate counting regions. Given the layered organization of SC and the expansion of the layers toward the dorsal surface, this radial sampling method was preferred to a fixed-distance grid method, allowing accurate analysis of density changes in the radial dimension (across layers) in the most reliable way.

Each counting rectangle included two exclusion lines (left and bottom) and two inclusion lines (right and top) (Atapour et al., 2017). A cell was counted if it was completely within the counting rectan-

gle or if the cell body touched the inclusion lines (Atapour et al., 2017). Neurons were identified within each sampling frame using previously published criteria (Atapour et al., 2017, 2019; Schmitz & Hof, 2005), and only cells with clear nuclei were counted, independent of size and shape. In calculating the number of cells per volume unit, both the section thickness ($40 \mu\text{m}$) and a shrinkage factor of 0.801 (Atapour et al., 2017) were considered. Average data from three consecutive sections through the central part of the SC were combined to calculate the mean neuronal density of NeuN-, CB-, CR- and PV-expressing neurons across SC layers, presented in Figures 2 and 4. For analysis of a rostrocaudal gradient (Figure 3), sampling frames were only placed in the central part of each coronal section, covering the middle two radial columns, as shown in Figure 1 (top right). Sections spaced at $400 \mu\text{m}$ were used for this analysis. The most caudal or rostral sections, which do not include all SC layers, were excluded. All statistical analyses were conducted using GraphPad Prism v9.2.0 (Graph-Pad Software, La Jolla, CA, USA).

3 | RESULTS

The approximate limits of the SC layers in the marmoset monkey were identified by convergent information from sections stained for

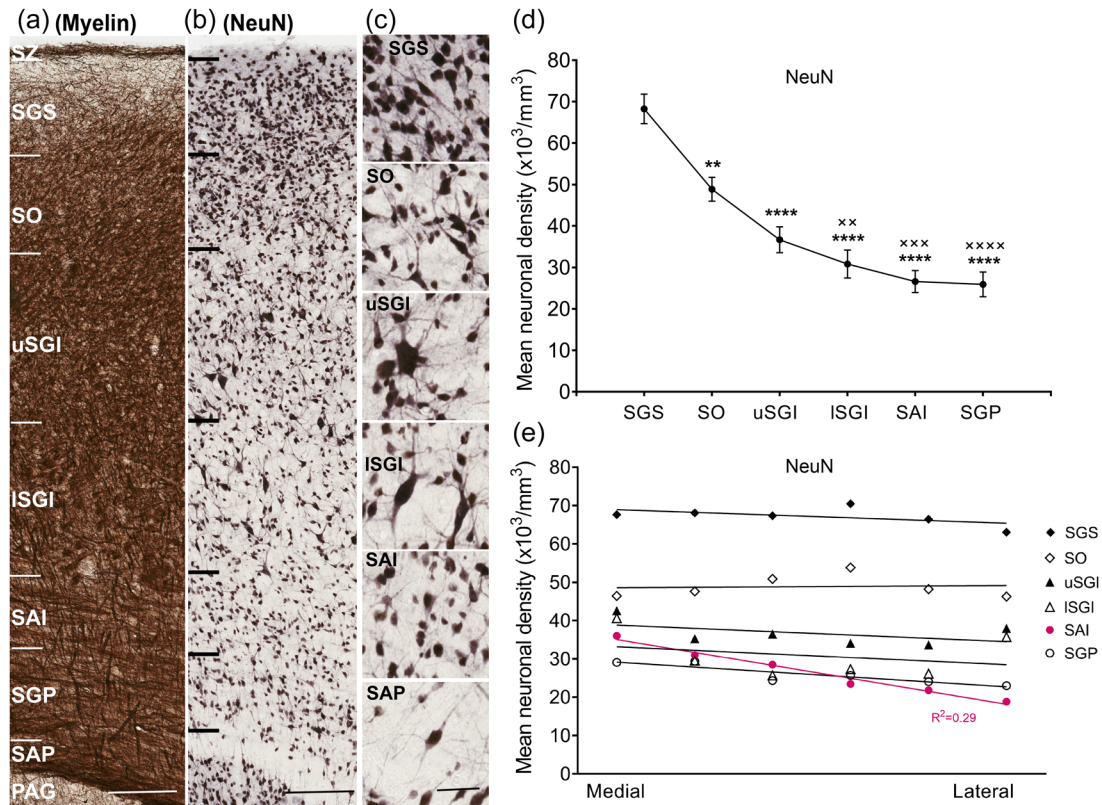


FIGURE 2 Neuronal density across superior colliculus (SC) layers. Representative close-up strips of marmoset SC layers after staining for myelin (a) and NeuN (b), scale: $200\ \mu\text{m}$. (c) Morphological types of NeuN-stained neurons shown at higher magnification, scale: $50\ \mu\text{m}$. (d) Mean neuronal density for the different SC layers (mean \pm SEM). Statistical comparisons: ** $p < .01$, **** $p < .0001$ for comparisons with SGS; xx $p < .01$, xxx $p < .001$, xxxxp $< .0001$ for comparison with SO. (e) Mean neuronal density across the mediolateral extent of each SC layer. With the exception of the SAI (red; $R^2 = 0.29$), most layers showed nonsignificant gradients in the mediolateral dimension. Layer abbreviations as in Figure 1

different neuronal markers. The dorsal-most layer was identified as the myelin-rich, thin SZ, followed by the SGS, which was characterized by a densely packed neuronal population in both the NeuN and CB stains and appeared to be more myelinated toward its lower limit (Figure 1). A pattern of alternating cell-rich and cell-poor regions was observed within the SO in the NeuN stain (Figure 1), which along with the ingress of myelinated fibers helped identify its borders. The presence of large cells was a hallmark of SGI, which could be divided into the upper and lower parts based on neuronal density. The transition from the SGI to the SAI was well characterized by a more uniform presence of smaller neurons. A horizontal fiber pattern specific to the SGP was evident with myelin and PV stains. SAP was thin, stained darkly for myelin, and contained few neurons as identified in NeuN stain.

3.1 | Gradient of neuronal density across layers in the SC

Neuronal morphology and density were variable among layers of SC, as identified using NeuN stain (Figure 2a,b). Examples of neurons present in different layers are shown in Figure 2c. NeuN, which specifically stains neurons (Wolf et al., 1996), revealed a clear gradient of density across the dorsoventral axis of the SC, with the highest concentra-

tion in the SGS and SO, as confirmed by one-way analysis of variance (ANOVA; Figure 2b,d; $F(5, 48) = 25.63, p < .0001$, post hoc; SGS vs. SO, $p < .01$, SGS vs. all other layers, $p < .0001$, SO vs. ISGI, $p < .01$, SO vs. SAI, $p < .001$ and SO vs. SGP, $p < .0001$). This analysis showed no significant difference between neuronal density in the intermediate and deep layers ($p > .05$). Neuronal density was mostly uniform across the mediolateral extent of the SC, with the only notable gradient being observed in the SAI (simple linear regression; $R^2 = 0.29, p < .0001$, Figure 2e). In summary, these results show that layers closer to the surface of the SC had higher neuronal densities compared to deeper layers, and that the distribution of neurons across the mediolateral axis of each layer was generally uniform, apart from in the SAI.

3.2 | Rostrocaudal gradient of neuronal density in the SC

Neuronal density in the SC gradually increased from rostral to caudal levels. This gradient of density was significantly different from zero for all layers of SC (Figure 3a-d, linear regression analysis; SGS; $R^2 = 0.60, p < .01$, SO; $R^2 = 0.77, p < .0001$, uSGI and ISGI; $R^2 = 0.59, p < .01$, SAI; $R^2 = 0.57, p < .01$, SGP; $R^2 = 0.38, p < .05$). However, there were no significant differences between the slopes obtained for the different layers ($F(5,72) = 2.21, p = .06$).

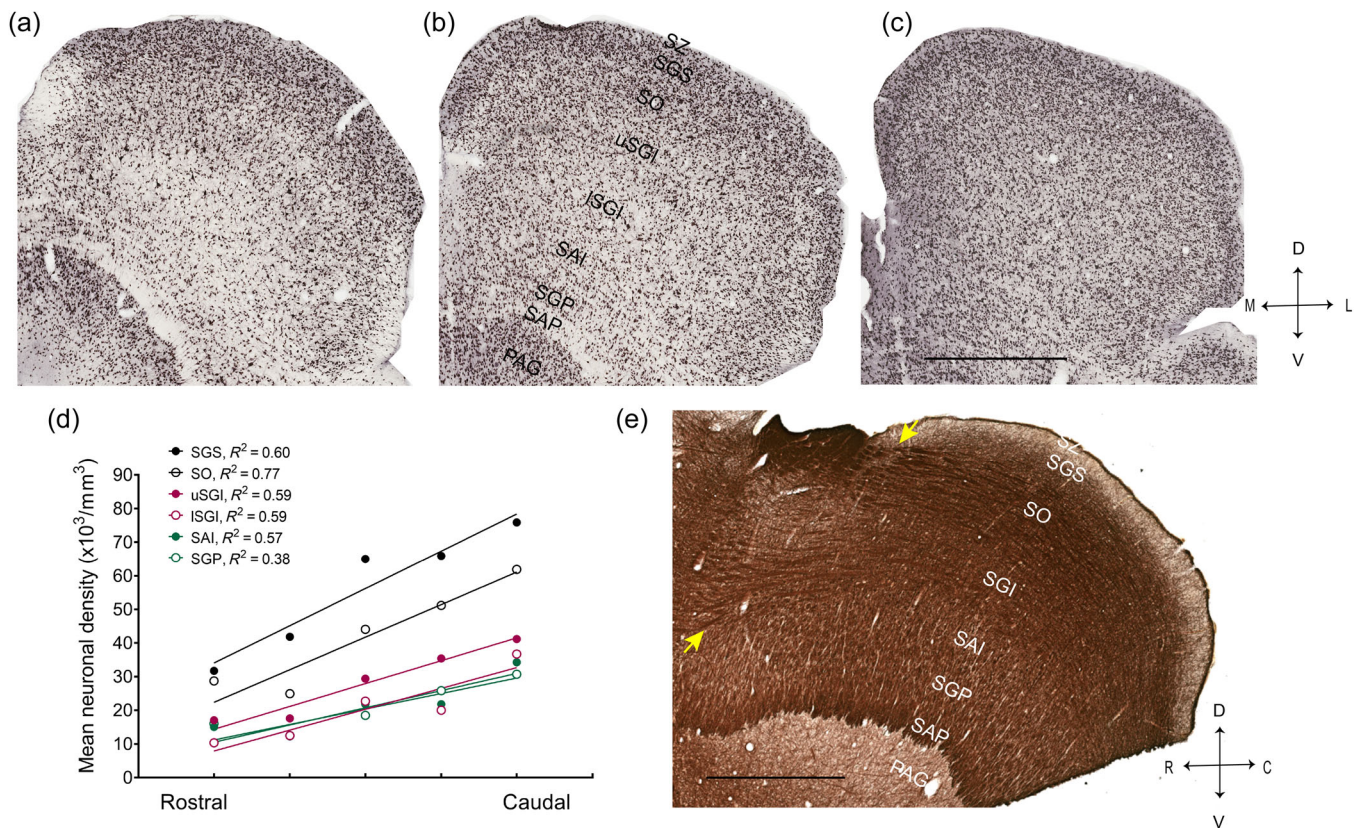


FIGURE 3 Neuronal density across the rostrocaudal dimension of the superior colliculus (SC). A change in density is clear in NeuN-stained images of marmoset SC, representing sections from interaural level +1.50 mm (a), +0.50 mm (b), and -2.0 mm (c) based on Paxinos et al. (2012). (d) Mean rostrocaudal gradient of density for all layers of the SC. (e) Representative image of myelin-stained, parasagittal section of the SC, taken from an animal not used for quantitative analysis in this study. Yellow arrows show points of entry of large fiber bundles into the rostral end. These bundles become progressively less obvious toward the caudal end. Layer abbreviations as in Figure 1. Abbreviations: C: caudal; D: dorsal; R, rostral; V, ventral. Scale: 1 mm

3.3 | Distribution of calcium-binding proteins in the SC

The cell bodies of neurons stained for CB, CR, and PV varied between 5 and 40 μm in diameter. Most CB-expressing neurons tended to be small and bipolar in shape (Figure 4a,b). Among those positive for CB were neurogliaform (NG) neurons (Overstreet-Wadiche & McBain, 2015), which were located mostly in the SGS and uSGI (Figure 4a,b, red arrow in 4b points to an NG neuron). These NG neurons, characterized by a cell body surrounded by a “halo” of thin processes, were also previously reported to be present in the CB-stained marmoset cortex (Bourne et al., 2007). CR-positive neurons were mostly small and bipolar, although some were among the largest neurons of the SC and had multipolar morphology (Figure 4b). PV-positive morphology ranged between unipolar, bipolar, and multipolar and was variable in size.

Staining for the three calcium-binding proteins revealed differential gradients of density across the dorsoventral axis of the SC (Figures 1 and 4a,c). The change in density was most obvious with CB staining, as CB-expressing neurons were mostly concentrated near the surface, particularly in the SGS, creating a superficial dense tier, followed by

a second tier in the SO and SGI and a third tier in the most ventral layers. This tiered appearance of CB stain best resembled those described for macaque monkeys (McHaffie et al., 2001) and resembled a series of stepwise decreases in neuronal density (Figure 4c). The pattern of decrease in density for CR-expressing neurons was similar to CB-expressing neurons, although the gradient of density was less pronounced because CR-expressing neurons were approximately twice as common as CB-expressing neurons in layers outside the SGS. The gradient of density for PV-expressing neurons was also less pronounced due to the relative paucity of these neurons in the upper layers.

Statistical comparison of mean neuronal densities using one-way ANOVA for CB, CR, and PV-expressing neurons showed significant differences between layers (CB: $F(5, 48) = 23.65, p < .0001$, PV: $F(5, 48) = 5.32, p < .001$, CR: $[F(5, 48) = 3.62, p < .01$, Figure 4c). For CB-expressing neurons, post hoc Tukey's test revealed statistically significant differences in mean neuronal density between the SGS and the remaining layers ($p < .0001$ for all comparisons). For PV-expressing neurons, a post hoc test revealed statistically significant differences between SGS or SO compared to deeper layers (Figure 4c, SGS vs. ISGI, $p < .05$, SGS vs. SAI or SGP, $p < .01$, SO vs. SGP, $p < .05$). However, for

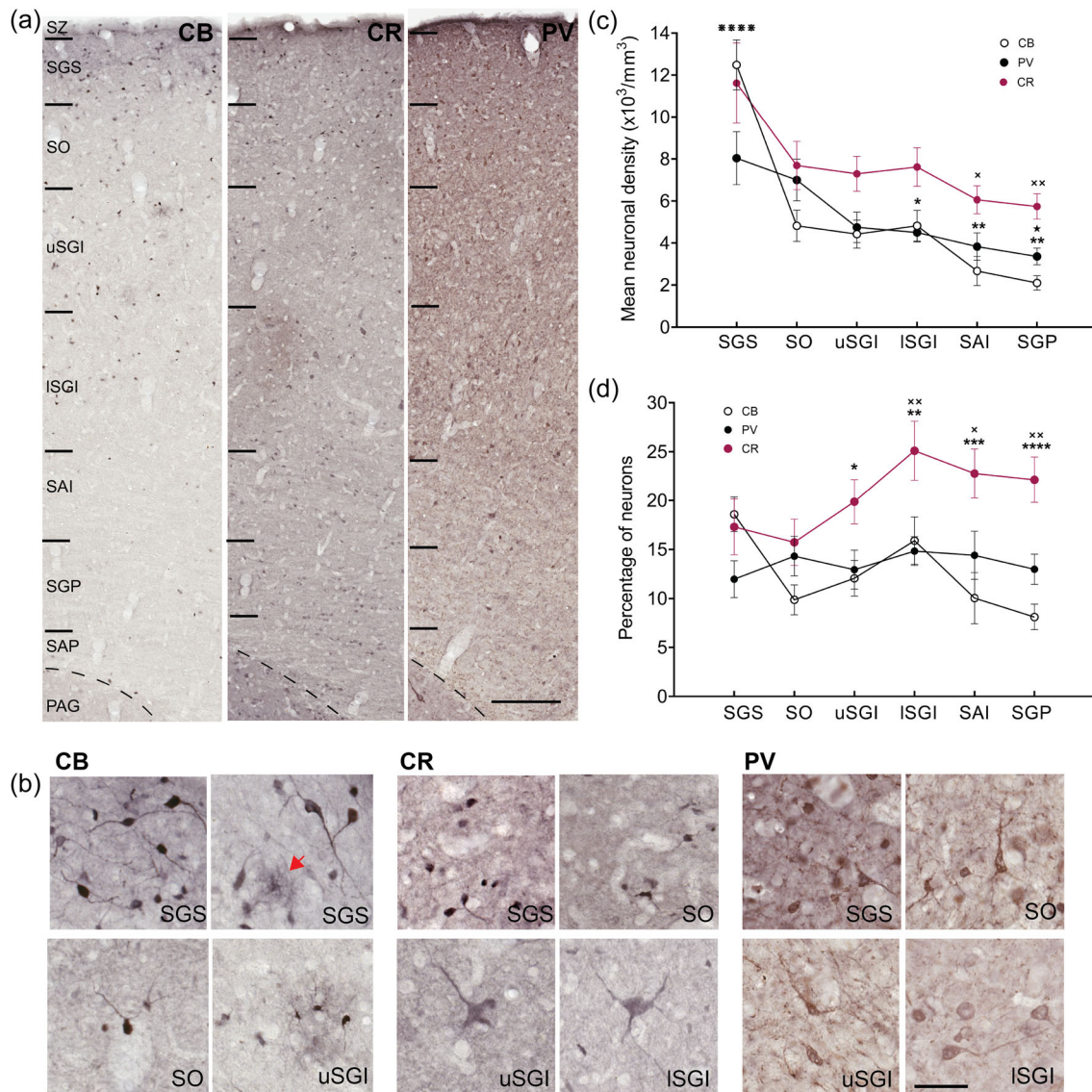


FIGURE 4 Differential expression of the calcium-binding proteins calbindin (CB), calretinin (CR), and parvalbumin (PV) in the marmoset superior colliculus (SC). (a) Representative close-up strips of marmoset SC layers stained for calcium-binding proteins, as indicated in Figure 1. Scale bar: 200 μ m. (b) Characteristic cellular morphologies observed in the SC after staining for CB, CR, and PV. The red arrow points to a CB-expressing neurogliaform neuron. Scale: 50 μ m. (c) Density of CB-, CR-, and PV-expressing neurons across the SC layers (mean \pm SEM). A decreasing trend was observed in the dorsoventral direction in all three stains. Statistical comparisons: **** p < .0001, for comparison of SGS with all other layers in CB staining; xp < .05, xxp < .01 for comparisons with SGS in CR staining; $*p$ < .05, $**p$ < .01 for comparison with SGS and $\star p$ < .05 for comparison with SO in PV staining. (d) Mean percentages of CB-, CR-, and PV-expressing neurons (relative to the density of NeuN-expressing neurons) within the SC. For comparisons within each layer; CR vs. CB, $*p$ < .05, $**p$ < .01, $***p$ < .001, $****p$ < .0001, and CR vs. PV, xp < .05, xxp < .01. Layer abbreviations as in Figure 1

CR-expressing neurons, a post hoc test revealed statistically significant differences only between SGS and the two deepest layers analyzed (Figure 4c, SGS vs. SAI, p < .05, SGS vs. SGP, p < .01, Figure 4c).

3.4 | Proportion of neurons stained for calcium-binding proteins

The proportions of CB-, CR-, and PV-expressing neurons (i.e., as a fraction of all neurons, identified by NeuN staining) are shown in Figure 4d.

Two-way ANOVA was performed to compare the ratio of CB-, CR-, and PV-expressing neurons across layers (type of calcium-binding protein: $F(2, 144) = 24.22$, p < .0001, layers: $F(5, 144) = 2.06$, $p = .07$, interaction: $F(10, 144) = 2.14$, $p = .025$). Post hoc analysis for comparison of the ratio of CB-, CR-, and PV-expressing neurons within each layer of the SC revealed statistically significant differences, suggesting a dominant presence of CR-expressing neurons compared to the other types in the deeper layers (Tukey's test: uSGI; CR vs. CB, p < .05, ISGI; CR vs. CB or PV, p < .01, SAI; CR vs. CB, p < .001 and CR vs. PV p < .05, SGP; CR vs. CB, p < .0001 and CR vs. PV p < .01, Figure 4d). Post hoc analysis for

comparison between layers in each stain showed that the proportion of CB-expressing neurons was significantly different between the SGS and SGP ($p < .05$), suggesting a decrease in the ratio of CB-expressing neurons toward the most ventral layer of SC. In contrast, the ratio of CR-expressing neurons showed a small increase toward the intermediate layers, and the difference between SO and ISGI was significantly different ($p < .05$). The proportion of PV-expressing neurons was nearly uniform across the dorsoventral axis, with no significant differences observed between layers ($p > .05$).

4 | DISCUSSION

We provide quantitative estimates of the total neuronal density in the different layers of the marmoset SC using stereological sampling applied to NeuN-immunostained sections. We also determined the distribution of neurons expressing different calcium-binding proteins and their percentages relative to estimates of total neuronal density.

4.1 | Neuronal density in different layers of the SC

This is the first quantitative study of the cellular composition of the marmoset SC. An earlier study on this species (Bourne & Rosa, 2003) described the morphological characteristics of neurons stained with the monoclonal antibody SMI-32, which recognizes non- and de-phosphorylated epitopes on the medium and heavy molecular weight subunits of the neurofilament protein (Sternberger & Sternberger, 1983) but did not include quantification. The present results support the findings of this study with regard to the laminar structure of the SC, which follows a relatively stereotyped mammalian pattern (Baldwin & Krubitzer, 2018; May, 2006; Rosa & Schmid, 1994; White & Munoz, 2012).

Although previous studies have estimated the neuronal density in the SC in other species (e.g., rats (Albers et al., 1988); hamsters (Ptacek & Fagan-Dubin, 1974); hemispherectomized green monkeys (Theoret et al., 2001), most of these studies were based on Nissl-stained sections, which tends to lead to overestimation (Atapour et al., 2019). The use of NeuN, a specific marker for neuronal nuclei, makes the present estimates more accurate. A quantification of neuronal density based on NeuN staining of the mouse SC (Tanaka et al., 2009) did not address laminar differences.

We found that neuronal density in the marmoset SC followed a dorsoventral laminar gradient, with the highest densities being observed in the superficial layers (SGS and SO), where neurons with small visual receptive fields are found (Tailby et al., 2012). In contrast, there was little variation along the mediolateral axis within the layers, which maps locations from upper to lower extrapersonal space (for review, see Rosa & Schmid, 1994). This is consistent with the functional organization of SC into layers that form superimposed functional maps aligned with the visual field representation (Isa et al., 2021; May, 2006) in which different points of the visual field are represented by approximately constant numbers of neurons (Capuano & McIlwain, 1981;

Rosa & Schmid, 1995). The higher density of neurons in sensory layers such as SGS and SO is in line with the more fine-grained representation, with each cell having smaller visual receptive fields compared with the deep layers (Cynader & Berman, 1972; Hubel et al., 1975; Rosa & Schmid, 1994), while lower neuronal density in the intermediate and deep layers fits with wider, multisensory and motor representations required for the integrative role of these neurons (Perrault et al., 2012; Robinson, 1972; Stein et al., 2001; White & Munoz, 2012). The requirement for a wider variety of axonal inputs from cortical and subcortical structures in the deeper layers can lead to more extensive dendritic arborization, which is linked to the presence of fewer neurons (for review, see Isa et al., 2021; May, 2006; White & Munoz, 2012). A similar principle governs the distributions of neurons across primary sensory and associative areas of the cortex (Atapour et al., 2019; Elston et al., 1999; Theodoni et al., 2021). Moreover, the more prominent occurrence of myelinated fiber bundles in the deep layers implies less space for the presence of neurons (May, 2006).

4.2 | Distribution of neuronal density across the rostrocaudal extent of SC

The existence of a neuronal density gradient across the rostrocaudal extent of the SC, which was present in every layer, is likely to be dictated by the amount of afferent fibers present. The point of entry of thick axonal bundles from the retina and cortex is in the rostral end of the SC (Figure 3e, May, 2006; White & Munoz, 2012). As these fibers make synapses en route to the caudal end, their density will become progressively lower, providing space for the presence of more closely packed neurons. While this pattern of white matter presence matches well with the observed gradient of neuronal density, particularly in the SO and SGI layers (which receive the bulk of fibers at point of entry; Figure 3e), other factors such as connectivity pattern with other subcortical structures could also contribute to this gradient of density.

4.3 | Distribution of neurons expressing calcium-binding proteins

The density of CB-expressing neurons followed a steep gradient from the superficial to deep layers of the SC, leading to a decrease in the proportion of CB-expressing neurons in the same direction. This observation in the marmoset SC agrees with most studies in primates, including those in the SC of *Cebus*, *titi*, and macaque monkeys (Baldwin & Krubitzer, 2018; Glezer et al., 1998; McHaffie et al., 2001; Mize & Luo, 1992; Soares et al., 2001). Indeed, the three-tiered arrangement for CB, described by McHaffie et al. (2001) in macaque monkeys, can also be observed in marmoset SC. The expression of PV followed a similar gradient as the overall neuronal density, and thus the proportion of these neurons remained constant across layers. The observed gradient of density for PV-expressing neurons, although less pronounced compared to CB-expressing neurons, was similar to observations in *titi* monkeys (Baldwin & Krubitzer, 2018). Studies in macaque and *Cebus*

monkeys, which reported a more uniform presence of PV-expressing neurons in all SC layers (Glezer et al., 1998; McHaffie et al., 2001; Soares et al., 2001), may have not captured the decreasing gradient of density observed in marmosets due to their qualitative nature. Indeed, our results with PV staining qualitatively resemble those reported previously for macaque monkeys (McHaffie et al., 2001).

Interestingly, the density of CR-expressing neurons showed less variation across the SC layers, thus leading to a higher proportion of such neurons in the intermediate layers. Similar to our findings, Soares et al. (2001) showed a higher presence of CR-expressing neurons in the intermediate layers in *Cebus* monkeys. The larger proportional representation of CR-expressing large neurons in the deeper layers of SC may be related to their integrative role, similar to the predominance of CR-expressing neurons in the frontal and parietal cortical areas of humans and monkeys (Conde et al., 1994; Džaja et al., 2014; Gabbott & Bacon, 1996; Ma et al., 2013). Evidence for the integrative role of CR-expressing neurons has been shown in many areas, including the cortex, olfactory bulb, and spinal cord (Hardy et al., 2018; Saffari et al., 2019; Smith et al., 2019; Su et al., 2021).

Our estimated ratios of CB- and CR-expressing neurons in the marmoset SC are similar to those reported in the macaque SC (Glezer et al., 1998). However, for PV-expressing neurons, our estimates are much lower. Differential expression of various calcium-binding proteins in SC neurons may underlie a particular compartmentalization aligned with their functional properties. Further understanding may depend on identifying the excitatory and/or inhibitory nature of these neurons, which can be addressed through future neurotransmitter colocalization studies.

Our density data for calcium-binding proteins have been obtained from the central part of the SC. While our qualitative observation suggests a similar pattern of staining across layers in the entire rostrocaudal extent of the SC, future quantitative studies may provide further insights into slight variations in the rostrocaudal distribution of these neurons, which could have implications for processing of sensory stimuli located nearly directly ahead of the animal versus in peripheral regions of the extrapersonal space.

Calcium-binding proteins exist in both excitatory and inhibitory neurons of the mammalian SC (Behan et al., 2002; Kang et al., 2002; Lee et al., 2006; Mize et al., 1991; Shang et al., 2018; Villalobos et al., 2018; Whyland et al., 2020). While such information is not available for the primate SC, it can be postulated that a similar relationship exists in primates, similar to other subcortical structures (Atapour et al., 2021; Felch & Van Hooser, 2012; Goodchild & Martin, 1998; Grubb & Thompson, 2004). The expression of calcium-binding proteins in subcortical nuclei, including the SC, has been shown to be subject to plastic modifications (Atapour et al., 2022; Gonzalez et al., 2005; Hada et al., 1999), and future studies may determine the significance of calcium-binding proteins as biomarkers for neuroplasticity within the SC, leading to further clarification of the role of this structure in functions such as residual vision (Atapour et al., 2021, 2022; Chan et al., 2021) and multisensory plasticity (Stein & Rowland, 2020; Yu et al., 2009) following cortical lesions.

ACKNOWLEDGMENTS

We acknowledge the contributions of the Monash Histology platform for slide scanning services and the Monash Animal Research Platform for the care of the animals involved in this study. This research was funded by a grant from the National Health and Medical Research Council (APP1194206) to Marcello G. P. Rosa.

Open access publishing facilitated by Monash University, as part of the Wiley - Monash University agreement via the Council of Australian University Librarians.

CONFLICT OF INTEREST

The authors declare no conflict of interest.

DATA AVAILABILITY STATEMENT

The data that support the findings of this study are available from the corresponding author upon reasonable request.

ORCID

Melissa H. Y. Chong  <https://orcid.org/0000-0001-6990-8277>

Katrina H. Worthy  <https://orcid.org/0000-0001-9539-9744>

Marcello G. P. Rosa  <https://orcid.org/0000-0002-6620-6285>

Nafiseh Atapour  <https://orcid.org/0000-0002-8773-9283>

REFERENCES

- Albers, F. J., Meek, J., & Nieuwenhuys, R. (1988). Morphometric parameters of the superior colliculus of albino and pigmented rats. *The Journal of Comparative Neurology*, 274(3), 357–370. <https://doi.org/10.1002/cne.902740306>
- Allen, K. M., Lawlor, J., Salles, A., & Moss, C. F. (2021). Orienting our view of the superior colliculus: Specializations and general functions. *Current opinion in neurobiology*, 71, 119–126. <https://doi.org/10.1016/j.conb.2021.10.005>
- Atapour, N., Worthy, K. H., Lui, L. L., Yu, H. H., & Rosa, M. G. P. (2017). Neuronal degeneration in the dorsal lateral geniculate nucleus following lesions of primary visual cortex: Comparison of young adult and geriatric marmoset monkeys. *Brain Structure & Function*, 222(7), 3283–3293. <https://doi.org/10.1007/s00429-017-1404-4>
- Atapour, N., Majka, P., Wolkowicz, I. H., Malamanova, D., Worthy, K. H., & Rosa, M. G. P. (2019). Neuronal distribution across the cerebral cortex of the marmoset monkey (*Callithrix jacchus*). *Cerebral Cortex*, 29(9), 3836–3863. <https://doi.org/10.1093/cercor/bhy263>
- Atapour, N., Worthy, K. H., & Rosa, M. G. P. (2021). Neurochemical changes in the primate lateral geniculate nucleus following lesions of striate cortex in infancy and adulthood: Implications for residual vision and blindsight. *Brain Structure & Function*, 226(9), 2763–2775. <https://doi.org/10.1007/s00429-021-02257-0>
- Atapour, N., Worthy, K. H., & Rosa, M. G. P. (2022). Remodeling of lateral geniculate nucleus projections to extrastriate area MT following long-term lesions of striate cortex. *Proceedings of the National Academy of Sciences of the United States of America*, 119(4), e2117137119. <https://doi.org/10.1073/pnas.2117137119>
- Baldwin, M. K. L., & Krubitzer, L. (2018). Architectonic characteristics of the visual thalamus and superior colliculus in titi monkeys. *The Journal of Comparative Neurology*, 526(11), 1760–1776. <https://doi.org/10.1002/cne.24445>
- Behan, M., Steinhacker, K., Jeffrey-Borger, S., & Meredith, M. A. (2002). Chemoarchitecture of GABAergic neurons in the ferret superior colliculus. *The Journal of Comparative Neurology*, 452(4), 334–359. <https://doi.org/10.1002/cne.10378>

- Bischof, D. P., Orduz, D., Lambot, L., Schiffmann, S. N., & Gall, D. (2012). Control of neuronal excitability by calcium binding proteins: A new mathematical model for striatal fast-spiking interneurons. *Frontiers In Molecular Neuroscience*, 5, 78. <https://doi.org/10.3389/fnmol.2012.00078>
- Bourne, J. A., & Rosa, M. G. P. (2003). Laminar expression of neurofilament protein in the superior colliculus of the marmoset monkey (*Callithrix jacchus*). *Brain Research*, 973(1), 142–145. [https://doi.org/10.1016/S0006-8993\(03\)02527-7](https://doi.org/10.1016/S0006-8993(03)02527-7)
- Bourne, J. A., Warner, C. E., Upton, D. J., & Rosa, M. G. P. (2007). Chemoarchitecture of the middle temporal visual area in the marmoset monkey (*Callithrix jacchus*): Laminar distribution of calcium-binding proteins (calbindin, parvalbumin) and nonphosphorylated neurofilament. *The Journal of Comparative Neurology*, 500(5), 832–849. <https://doi.org/10.1002/cne.21190>
- Capuano, U., & McIlwain, J. T. (1981). Reciprocity of receptive field images and point images in the superior colliculus of the cat. *The Journal of Comparative Neurology*, 196(1), 13–23. <https://doi.org/10.1002/cne.901960103>
- Chan, J. M., Worthy, K. H., Rosa, M. G. P., Reser, D. H., & Atapour, N. (2021). Volume reduction without neuronal loss in the primate pulvinar complex following striate cortex lesions. *Brain Structure & Function*, 226(7), 2417–2430. <https://doi.org/10.1007/s00429-021-02345-1>
- Chen, C. Y., Hoffmann, K. P., Distler, C., & Hafed, Z. M. (2019). The foveal visual representation of the primate superior colliculus. *Current Biology*, 29(13), 2109–2119 e2107. <https://doi.org/10.1016/j.cub.2019.05.040>
- Conde, F., Lund, J. S., Jacobowitz, D. M., Baimbridge, K. G., & Lewis, D. A. (1994). Local circuit neurons immunoreactive for calretinin, calbindin D-28k or parvalbumin in monkey prefrontal cortex: Distribution and morphology. *The Journal of Comparative Neurology*, 341(1), 95–116. <https://doi.org/10.1002/cne.903410109>
- Corneil, B. D., & Munoz, D. P. (2014). Overt responses during covert orienting. *Neuron*, 82(6), 1230–1243. <https://doi.org/10.1016/j.neuron.2014.05.040>
- Cynader, M., & Berman, N. (1972). Receptive-field organization of monkey superior colliculus. *Journal of Neurophysiology*, 35(2), 187–201. <https://doi.org/10.1152/jn.1972.35.2.187>
- Džaja, D., Hladnik, A., Bičanić, I., Baković, M., & Petanjek, Z. (2014). Neocortical calretinin neurons in primates: Increase in proportion and microcircuitry structure. *Frontiers in Neuroanatomy*, 8, 103. <https://doi.org/10.3389/fnana.2014.00103>
- Elston, G. N., Tweedale, R., & Rosa, M. G. (1999). Cellular heterogeneity in cerebral cortex: a study of the morphology of pyramidal neurons in visual areas of the marmoset monkey. *The Journal of comparative neurology*, 415(1), 33–51. [https://doi.org/10.1002/\(sici\)1096-9861\(19991206\)415:1<33::aid-cne3>3.0.co;2-m](https://doi.org/10.1002/(sici)1096-9861(19991206)415:1<33::aid-cne3>3.0.co;2-m)
- Essig, J., Hunt, J. B., & Felsen, G. (2021). Inhibitory neurons in the superior colliculus mediate selection of spatially-directed movements. *Communications Biology*, 4(1), 719. <https://doi.org/10.1038/s42003-021-02248-1>
- Felch, D. L., & Van Hooser, S. D. (2012). Molecular compartmentalization of lateral geniculate nucleus in the gray squirrel (*Sciurus carolinensis*). *Frontiers in Neuroanatomy*, 6, 12. <https://doi.org/10.3389/fnana.2012.00012>
- Finlay, B. L., Charvet, C. J., Bastille, I., Cheung, D. T., Muniz, J. A., & de Lima Silveira, L. C. (2014). Scaling the primate lateral geniculate nucleus: niche and neurodevelopment in the regulation of magnocellular and parvocellular cell number and nucleus volume. *The Journal of Comparative Neurology*, 522(8), 1839–1857. <https://doi.org/10.1002/cne.23505>
- Gabbott, P. L., & Bacon, S. J. (1996). Local circuit neurons in the medial prefrontal cortex (areas 24a,b,c, 25 and 32) in the monkey: II. Quantitative areal and laminar distributions. *The Journal of Comparative Neurology*, 364(4), 609–636. [https://doi.org/10.1002/\(SICI\)1096-9861\(19960122\)364:4609::AID-CNE23.0.CO;2-7](https://doi.org/10.1002/(SICI)1096-9861(19960122)364:4609::AID-CNE23.0.CO;2-7)
- Gallyas, F. (1979). Silver staining of myelin by means of physical development. *Neurological Research*, 1(2), 203–209. <https://doi.org/10.1080/01616412.1979.11739553>
- Glezer, I. I., Hof, P. R., & Morgane, P. J. (1998). Comparative analysis of calcium-binding protein-immunoreactive neuronal populations in the auditory and visual systems of the bottlenose dolphin (*Tursiops truncatus*) and the macaque monkey (*Macaca fascicularis*). *Journal of Chemical Neuroanatomy*, 15(4), 203–237. [https://doi.org/10.1016/S0891-0618\(98\)00022-2](https://doi.org/10.1016/S0891-0618(98)00022-2)
- Gonzalez, D., Satriotomo, I., Miki, T., Lee, K. Y., Yokoyama, T., Touge, T., Matsumoto, Y., Li, H. P., Kuriyama, S., & Takeuchi, Y. (2005). Effects of monocular enucleation on calbindin-D 28k and c-Fos expression in the lateral geniculate nucleus in rats. *Okajimas Folia Anatomica Japonica*, 82(1), 9–18. <https://doi.org/10.2535/ofaj.82.9>
- Goodchild, A. K., & Martin, P. R. (1998). The distribution of calcium-binding proteins in the lateral geniculate nucleus and visual cortex of a New World monkey, the marmoset, *Callithrix jacchus*. *Visual Neuroscience*, 15(4), 625–642. <https://doi.org/10.1017/S0952523898154044>
- Grubb, M. S., & Thompson, I. D. (2004). Biochemical and anatomical subdivision of the dorsal lateral geniculate nucleus in normal mice and in mice lacking the beta2 subunit of the nicotinic acetylcholine receptor. *Vision Research*, 44(28), 3365–3376. <https://doi.org/10.1016/j.visres.2004.09.003>
- Hada, Y., Yamada, Y., Imamura, K., Mataga, N., Watanabe, Y., & Yamamoto, M. (1999). Effects of monocular enucleation on parvalbumin in rat visual system during postnatal development. *Investigative Ophthalmology & Visual Science*, 40(11), 2535–2545.
- Hardy, D., Malvaut, S., Breton-Provencher, V., & Saghatelian, A. (2018). The role of calretinin-expressing granule cells in olfactory bulb functions and odor behavior. *Scientific Reports*, 8(1), 9385. <https://doi.org/10.1038/s41598-018-27692-8>
- Hilbig, H., Bidmon, H. J., Zilles, K., & Busecke, K. (1999). Neuronal and glial structures of the superficial layers of the human superior colliculus. *Anatomy and Embryology*, 200(1), 103–115. <https://doi.org/10.1007/s004290050264>
- Hubel, D. H., LeVay, S., & Wiesel, T. N. (1975). Mode of termination of retinotectal fibers in macaque monkey: An autoradiographic study. *Brain Research*, 96(1), 25–40. [https://doi.org/10.1016/0006-8993\(75\)90567-3](https://doi.org/10.1016/0006-8993(75)90567-3)
- Isa, T., Marquez-Legorreta, E., Grillner, S., & Scott, E. K. (2021). The tectum/superior colliculus as the vertebrate solution for spatial sensory integration and action. *Current Biology*, 31(11), R741–R762. <https://doi.org/10.1016/j.cub.2021.04.001>
- Kang, Y. S., Kong, J. H., Park, W. M., Kwon, O. J., Lee, J. E., Kim, S. Y., & Jeon, C. J. (2002). Morphology of calretinin-immunoreactive neurons in the superficial layers of hamster superior colliculus after enucleation: Lack of co-localization with GABA. *Molecules and Cells*, 14(3), 361–366.
- Kook, S. Y., Jeong, H., Kang, M. J., Park, R., Shin, H. J., Han, S. H., Son, S. M., Song, H., Baik, S. H., Moon, M., Yi, E. C., Hwang, D., & Mook-Jung, I. (2014). Crucial role of calbindin-D28k in the pathogenesis of Alzheimer's disease mouse model. *Cell Death and Differentiation*, 21(10), 1575–1587. <https://doi.org/10.1038/cdd.2014.67>
- Laemle, L. K. (1981). A Golgi study of cellular morphology in the superficial layers of superior colliculus man, Saimiri, and Macaca. *Journal fur Hirnforschung*, 22(3), 253–263.
- Lee, J. Y., Choi, J. S., Ahn, C. H., Kim, I. S., Ha, J. H., & Jeon, C. J. (2006). Calcium-binding protein calretinin immunoreactivity in the dog superior colliculus. *Acta Histochemica et Cytochemica*, 39(5), 125–138. <https://doi.org/10.1267/ahc.06008>
- Ma, T. P., Cheng, H. W., Czech, J. A., & Rafols, J. A. (1990). Intermediate and deep layers of the macaque superior colliculus: A Golgi study. *The Journal of Comparative Neurology*, 295(1), 92–110. <https://doi.org/10.1002/cne.902950109>
- Ma, T., Wang, C., Wang, L., Zhou, X., Tian, M., Zhang, Q., Zhang, Y., Li, J., Liu, Z., Cai, Y., Liu, F., You, Y., Chen, C., Campbell, K., Song, H., Ma, L., Rubenstein,

- J. L., & Yang, Z. (2013). Subcortical origins of human and monkey neocortical interneurons. *Nature Neuroscience*, 16(11), 1588–1597. <https://doi.org/10.1038/nn.3536>
- Majka, P., Bai, S., Bakola, S., Bednarek, S., Chan, J. M., Jermakow, N., Passarelli, L., Reser, D. H., Theodoni, P., Worthy, K. H., Wang, X. J., Wójcik, D. K., Mitra, P. P., & Rosa, M. G. P. (2020). Open access resource for cellular-resolution analyses of corticocortical connectivity in the marmoset monkey. *Nature Communications*, 11(1), 1133. <https://doi.org/10.1038/s41467-020-14858-0>
- Majka, P., Chaplin, T. A., Yu, H. H., Tolpygo, A., Mitra, P. P., Wójcik, D. K., & Rosa, M. G. P. (2016). Towards a comprehensive atlas of cortical connections in a primate brain: Mapping tracer injection studies of the common marmoset into a reference digital template. *The Journal of Comparative Neurology*, 524(11), 2161–2181. <https://doi.org/10.1002/cne.24023>
- May, P. J. (2006). The mammalian superior colliculus: Laminar structure and connections. *Progress in Brain Research*, 151, 321–378. [https://doi.org/10.1016/S0079-6123\(05\)51011-2](https://doi.org/10.1016/S0079-6123(05)51011-2)
- McHaffie, J. G., Anstrom, K. K., Gabriele, M. L., & Stein, B. E. (2001). Distribution of the calcium-binding proteins calbindin D-28K and parvalbumin in the superior colliculus of adult and neonatal cat and rhesus monkey. *Experimental Brain Research*, 141(4), 460–470. <https://doi.org/10.1007/s00221-001-0908-5>
- Mitchell, J. F., & Leopold, D. A. (2015). The marmoset monkey as a model for visual neuroscience. *Neuroscience Research*, 93, 20–46. <https://doi.org/10.1016/j.neures.2015.01.008>
- Mize, R. R. (1992). The organization of GABAergic neurons in the mammalian superior colliculus. *Progress in Brain Research*, 90, 219–248. [https://doi.org/10.1016/s0079-6123\(08\)63616-x](https://doi.org/10.1016/s0079-6123(08)63616-x)
- Mize, R. R., Jeon, C. J., Butler, G. D., Luo, Q., & Emson, P. C. (1991). The calcium binding protein calbindin-D 28K reveals subpopulations of projection and interneurons in the cat superior colliculus. *The Journal of Comparative Neurology*, 307(3), 417–436. <https://doi.org/10.1002/cne.903070307>
- Mize, R. R., & Luo, Q. (1992). Visual deprivation fails to reduce calbindin 28kD or GABA immunoreactivity in the rhesus monkey superior colliculus. *Visual Neuroscience*, 9(2), 157–168. <https://doi.org/10.1017/s0952523800009627>
- Paxinos, G., Watson, C., Petrides, M., Rosa, M. G. P., & Tokuno, H. (2012). *The Marmoset Brain in Stereotaxic Coordinates*. San Diego: Academic Press.
- Okano, H., Hikishima, K., Iriki, A., & Sasaki, E. (2012). The common marmoset as a novel animal model system for biomedical and neuroscience research applications. *Seminars In Fetal & Neonatal Medicine*, 17(6), 336–340. <https://doi.org/10.1016/j.siny.2012.07.002>
- Overstreet-Wadiche, L., & McBain, C. J. (2015). Neurogliaform cells in cortical circuits. *Nature reviews. Neuroscience*, 16(8), 458–468. <https://doi.org/10.1038/nrn3969>
- Perrault, T. J. Jr., Rowland, B. A., & Stein, B. E. (2012). The organization and plasticity of multisensory integration in the midbrain. In Murray, M. M., Wallace M. T. (Eds.), *The neural bases of multisensory processes*. CRC Press/Taylor & Francis, 15, 279–300.
- Ptacek, J. M., & Fagan-Dubin, L. (1974). Developmental changes in neuron size and density in the visual cortex and superior colliculus of the postnatal golden hamster. *The Journal of Comparative Neurology*, 158(3), 237–242. <https://doi.org/10.1002/cne.901580302>
- Robinson, D. A. (1972). Eye movements evoked by collicular stimulation in the alert monkey. *Vision Research*, 12(11), 1795–1808. [https://doi.org/10.1016/0042-6989\(72\)90070-3](https://doi.org/10.1016/0042-6989(72)90070-3)
- Rosa, M. G. P., & Schmid, L. M. (1994). Topography and extent of visual-field representation in the superior colliculus of the megachiropteran *Pteropus*. *Visual Neuroscience*, 11(6), 1037–57. <https://doi.org/10.1017/s0952523800006878>
- Rosa, M. G. P., & Schmid, L. M. (1995). Magnification factors, receptive field images and point-image size in the superior colliculus of flying foxes: Comparison with the primary visual cortex. *Experimental Brain Research*, 102(3), 551–556. <https://doi.org/10.1007/bf00230660>
- Saffari, R., Grotefeld, K., Kravchenko, M., Zhang, M., & Zhang, W. (2019). Calretinin(+)-neurons-mediated GABAergic inhibition in mouse prefrontal cortex. *Progress in Neuro-Psychopharmacology & Biological Psychiatry*, 94, 109658. <https://doi.org/10.1016/j.pnpbp.2019.109658>
- Schmitz, C., & Hof, P. R. (2005). Design-based stereology in neuroscience. *Neuroscience*, 130(4), 813–831. <https://doi.org/10.1016/j.neuroscience.2004.08.050>
- Shang, C., Chen, Z., Liu, A., Li, Y., Zhang, J., Qu, B., Yan, F., Zhang, Y., Liu, W., Liu, Z., Guo, X., Li, D., Wang, Y., & Cao, P. (2018). Divergent midbrain circuits orchestrate escape and freezing responses to looming stimuli in mice. *Nature Communications*, 9(1), 1232. <https://doi.org/10.1038/s41467-018-03580-7>
- Smith, K. M., Browne, T. J., Davis, O. C., Coyle, A., Boyle, K. A., Watanabe, M., Dickinson, S. A., Iredale, J. A., Gradwell, M. A., Jobling, P., Callister, R. J., Dayas, C. V., Hughes, D. I., & Graham, B. A. (2019). Calretinin positive neurons form an excitatory amplifier network in the spinal cord dorsal horn. *eLife*, 8, e49190. <https://doi.org/10.7554/eLife.49190>
- Soares, J. G., Botelho, E. P., & Gattass, R. (2001). Distribution of calbindin, parvalbumin and calretinin in the lateral geniculate nucleus and superior colliculus in Cebus apella monkeys. *Journal of Chemical Neuroanatomy*, 22(3), 139–146. [https://doi.org/10.1016/s0891-0618\(01\)00123-5](https://doi.org/10.1016/s0891-0618(01)00123-5)
- Solomon, S. G., & Rosa, M. G. P. (2014). A simpler primate brain: The visual system of the marmoset monkey. *Frontiers in Neural Circuits*, 8, 96. <https://doi.org/10.3389/fncir.2014.00096>
- Sooksawate, T., Isa, K., Behan, M., Yanagawa, Y., & Isa, T. (2011). Organization of GABAergic inhibition in the motor output layer of the superior colliculus. *The European Journal of Neuroscience*, 33(3), 421–432. <https://doi.org/10.1111/j.1460-9568.2010.07535.x>
- Stein, B. E., Jiang, W., Wallace, M. T., & Stanford, T. R. (2001). Nonvisual influences on visual-information processing in the superior colliculus. *Progress in Brain Research*, 134, 143–156. [https://doi.org/10.1016/s0079-6123\(01\)34011-6](https://doi.org/10.1016/s0079-6123(01)34011-6)
- Stein, B. E., & Rowland, B. A. (2020). Using superior colliculus principles of multisensory integration to reverse hemianopia. *Neuropsychologia*, 141, 107413. <https://doi.org/10.1016/j.neuropsychologia.2020.107413>
- Sternberger, L. A., & Sternberger, N. H. (1983). Monoclonal antibodies distinguish phosphorylated and nonphosphorylated forms of neurofilaments in situ. *Proceedings of the National Academy of Sciences of the United States of America*, 80(19), 6126–6130. <https://doi.org/10.1073/pnas.80.19.6126>
- Su, M., Liu, J., Yu, B., Zhou, K., Sun, C., Yang, M., & Zhao, C. (2021). Loss of Calretinin in L5a impairs the formation of the barrel cortex leading to abnormal whisker-mediated behaviors. *Molecular Brain*, 14(1), 67. <https://doi.org/10.1186/s13041-021-00775-w>
- Tanaka, H., Ito, Y., Nakamura, S., Shimazawa, M., & Hara, H. (2009). Involvement of brain-derived neurotrophic factor in time-dependent neurodegeneration in the murine superior colliculus after intravitreal injection of N-methyl-D-aspartate. *Molecular Vision*, 15, 662–669. <https://www.ncbi.nlm.nih.gov/pubmed/19347051>
- Theodoni, P., Majka, P., Reser, D. H., Wójcik, D. K., Rosa, M. G. P., & Wang, X. J. (2021). Structural attributes and principles of the neocortical connectome in the marmoset monkey. *Cerebral Cortex*, 32(1), 15–28. <https://doi.org/10.1093/cercor/bhab191>
- Tailby, C., Cheong, S. K., Pietersen, A. N., Solomon, S. G., & Martin, P. R. (2012). Colour and pattern selectivity of receptive fields in superior colliculus of marmoset monkeys. *The Journal of Physiology*, 590(16), 4061–4077. <https://doi.org/10.1113/jphysiol.2012.230409>
- Theoret, H., Boire, D., Herbin, M., & Ptito, M. (2001). Anatomical sparing in the superior colliculus of hemispherectomized monkeys. *Brain Research*, 894(2), 274–280. [https://doi.org/10.1016/s0006-8993\(01\)02030-3](https://doi.org/10.1016/s0006-8993(01)02030-3)

- Villalobos, C. A., Wu, Q., Lee, P. H., May, P. J., & Basso, M. A. (2018). Parvalbumin and GABA microcircuits in the mouse superior colliculus. *Frontiers in Neural Circuits*, 12, 35. <https://doi.org/10.3389/fncir.2018.00035>
- White, B. J., & Munoz, D. P. (2012). The superior colliculus. In Livservedge, P. S., Gilchrist, I., & Everling, S. (Eds.), *Oxford handbook of eye movements* (pp. 195–213). Oxford University Press. <https://doi.org/10.1093/oxfordhb/9780199539789.013.0011>
- Williams, R. W., & Rakic, P. (1988). Three-dimensional counting: an accurate and direct method to estimate numbers of cells in sectioned material. *The Journal of Comparative Neurology*, 278(3), 344–352. <https://doi.org/10.1002/cne.902780305>
- Wolf, H. K., Buslei, R., Schmidt-Kastner, R., Schmidt-Kastner, P. K., Pietsch, T., Wiestler, O. D., & Blumcke, I. (1996). NeuN: A useful neuronal marker for diagnostic histopathology. *The Journal of Histochemistry and Cytochemistry*, 44(10), 1167–1171. <https://doi.org/10.1177/44.10.8813082>
- Worthy, K. H., Burman, K. J., & Rosa, M. G. P. (2017). *Gallyas silver stain for myelin*. The Marmoset Brain Connectivity Atlas Project. <https://doi.org/10.13140/RG.2.2.23807.76968>
- Whyland, K. L., Slusarczyk, A. S., & Bickford, M. E. (2020). GABAergic cell types in the superficial layers of the mouse superior colliculus. *The Journal of Comparative Neurology*, 528(2), 308–320. <https://doi.org/10.1002/cne.24754>
- Yu, L., Stein, B. E., & Rowland, B. A. (2009). Adult plasticity in multisensory neurons: Short-term experience-dependent changes in the superior colliculus. *The Journal of Neuroscience*, 29(50), 15910–15922. <https://doi.org/10.1523/JNEUROSCI.4041-09.2009>

How to cite this article: Chong, M. H. Y., Worthy, K. H., Rosa, M. G. P., & Atapour, N. (2022). Neuronal density and expression of calcium-binding proteins across the layers of the superior colliculus in the common marmoset (*Callithrix jacchus*). *Journal of Comparative Neurology*, 530, 2966–2976. <https://doi.org/10.1002/cne.25388>